Available online at www.sciencedirect.com
ScienceDirect
Cement and Concrete Research 37 (2007) 789–795
Cement and Concrete Research

Measurement of the coefficient of thermal expansion of ultra-high strength cementitious composites using fibre optic sensors

Paul Childs [a,*], Allan C.L. Wong [a], N. Gowripalan [b], G.D. Peng [a]

[a] School of Electrical Engineering, University of New South Wales, Sydney 2052, Australia
[b] School of Civil and Environmental Engineering, University of New South Wales, Sydney 2052, Australia

Received 7 November 2005; accepted 7 February 2007

Abstract

Fibre Bragg Grating (FBG) sensors were embedded into cement mortar and ultra-high strength reactive powder concrete (RPC) prisms. Thermal tests are performed to accurately characterise the coefficient of thermal expansion (CTE) of these prisms using the measured signals from the embedded sensors. With the use of the fibre optic sensors, the difficulties inherent in using conventional techniques, such as strain gauges or vibrating wire gauges, to measure the thermal properties of cementitious materials are overcome. The error values associated with the measurements, typically measured to be as low as ±0.04 με/K, are a full order of magnitude less than what is expected for standard conventional testing using a length comparator.

Keywords: Fibre optic sensors; Fibre Bragg gratings; Thermal expansion; CTE; Reactive powder concrete

1. Introduction

The coefficient of thermal expansion (CTE), despite being a very fundamental property, has seldom been reliably measured and characterised for cementitious materials. Conventional testing of thermal stresses and strains is limited in that there is a large amount of measurement error involved, making comparisons between results unreliable. A knowledge of the coefficient of thermal expansion of cementitious materials is of importance to modelling the thermal behaviour of the material. Excessive thermal stresses in cementitious materials can lead to cracking and spalling. Restrained thermal stresses have been shown to significantly increase the risk of explosive spalling of high performance concrete exposed to fire [1,2]. Being able to completely model the thermal stresses and strains within the material will mean that constraints can be applied during the design stage to adjust the material properties so as to bring them within an acceptable operating range.

One important area of research regarding the thermal properties of cementitious materials is that of fire damage. Usmani and co-workers at the University of Edinburgh have observed that the behaviour of fire damaged cementitious composites, in particular their robustness against collapse, widely deviates from what is expected from an analytical treatment. As a result more involved analytical modelling has been applied in order to attempt to describe the observed results. Nevertheless they say that "the exact mechanism of failure is still a matter for speculation" [3]. To be able to directly experimentally monitor the thermal effects occurring within the concrete elements as they are being subject to fire damage would go a long way to understanding the mechanisms of failure of fire damaged cementitious composites. Recently da Silva et al. have used fibre Bragg grating (FBG) sensors to monitor the fire damage on a concrete cantilever beam by means of dynamic analysis [4].

There are several difficulties involved in performing thermal expansion measurements on cementitious materials. The two conventional methods are to use electrical sensors or to take mechanical measurements [5,6] of the distance between two gauge points. For the case of the former of the two methods, the electrical gauges will become dysfunctional if the sample is placed in a liquid bath for heating. These gauges can be waterproofed, but this introduces added complications in

* Corresponding author.
E-mail address: p.childs@student.unsw.edu.au (P. Childs).

0008-8846/$ - see front matter © 2007 Elsevier Ltd. All rights reserved.
doi:10.1016/j.cemconres.2007.02.015

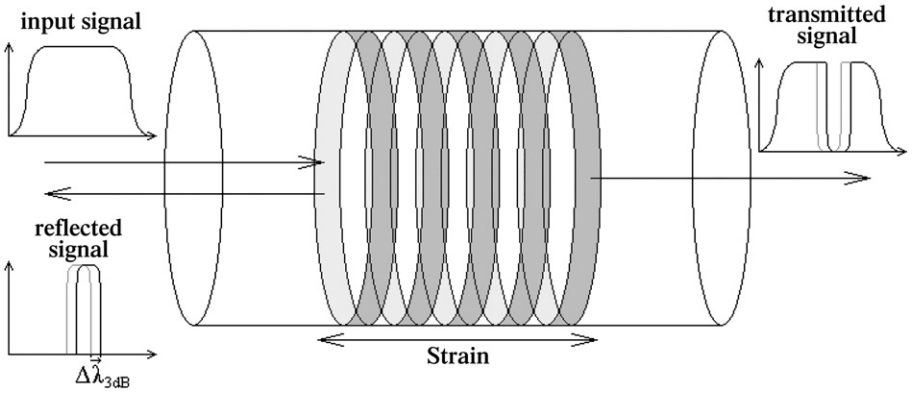

Fig. 1. FBG principle of operation.

calibrating the response of the sensors. The alternative option, namely performing the tests in an oven, is undesirable as, due to air having a lower thermal conductivity than that of water, the uniformity of the temperature distribution of an oven is poor compared to that of a water bath, and thus produces larger measurement errors. In order for the latter of the two conventional methods to be sufficiently accurate, a large distance is needed for the gauge length and hence a large sample is needed. This means that a large amount of time is needed to bring the sample to thermal equilibrium in order for accurate measurements to be made. If the sample is placed in a liquid bath, as is required for performing an accurate measurement, the experiment will either suffer from errors incurred from moving the sample between the liquid bath and the measurement apparatus or from the complicated calibration involved in the combined changes with temperature of the sample, measurement apparatus and liquid used for heating.

The specifications in [5,6] which make use of mechanical measurements calculate the linear coefficient of thermal expansion as:

$$C = \frac{(R_h - R_c)}{G\Delta T}, \tag{1}$$

where R_h and R_c are the length measurements for hot and cold temperatures respectively, G is the gauge length and ΔT is the change in temperature. The corresponding differential form of this equation is:

$$\frac{dC}{C} = \frac{d(R_h - R_c)}{(R_h - R_c)} - \frac{d\Delta T}{\Delta T} - \frac{dG}{G}. \tag{2}$$

ΔT is given as 55 °C and dΔT as 2.2 °C. d$(R_h - R_c)$ is given as $2 * 10^{-4}$ in. and taking the value of C to be roughly $1.2 * 10^{-5}$ K^{-1} and a value of G as 10 in. gives $(R_h - R_c)$ as $6.6 * 10^{-3}$ in. dG can be taken to be negligible compared to the other errors. Thus, with the aforementioned error involved in moving the sample to and from the measuring apparatus and heating/cooling baths excluded from consideration, the total relative error in C is calculated as 7%, hence there is often the need to make repeated measurements of many samples in order to statistically reduce the final error to an acceptable value.

An alternative to these conventional methods of testing is to use fibre optic sensors, which manage to overcome the difficulties mentioned so far. The elastic and thermal properties of the optical fibre can be measured extremely accurately and as such the error involved in calibrating fibre optic sensors is very small allowing accurate thermal testing to be performed. Reviews of the use of optical fibre sensors are given in [7,8].

To date optical fibre sensors have been used for a variety of applications in the field of civil engineering. A review of the status of early research is given in [9]. More recently, optical fibre sensors have been used in applications such as measuring early age shrinkage effects [10], field trials of monitoring prestress tendons [11], fibre reinforced polymer (FRP) layers and reinforced concrete beams and decks [12] as well as a recently commissioned reactive powder concrete (RPC) road bridge [13].

Typically, optical fibre is coated with an acrylate coating. This coating protects the fibre against damage from the typical stresses involved in its general handling. Unlike silica, it is resistant to alkali reactions and thus protects the fibre from breaking down when embedded into a cementitious host material. Other coating materials are also possible. For high temperature testing Silicon Carbide is a better material to use. Acrylate softens and begins to flow above the glass transition temperature of between 95 °C and 105 °C, above which the silica fibre can slip with respect to the host material, thus reducing the apparent amount of thermal strain. Silicon Carbide is also resistant to alkali reactions and does not flow like polymer coatings do. It also has the added benefit that it is transparent to the 5 eV UV light required for writing the FBGs meaning that the coating does not need to be removed when the fibre is exposed to the laser light, which extends the expected lifetime of the embedded sensor from the order of decades to the order of centuries as would be more appropriate for long term monitoring of large scale structures. The drawback of using a ceramic material like Silicon Carbide for coating the fibre is that it is difficult to remove the coating and to keep the fibre intact. This means that initial testing of the sensors is a lot more time consuming. Also due to the hardness of the material, it does not cushion the fibre against stress like polymer coatings do leading to enhanced microcracking through mishandling of the fibre. In

Table 1
Cement mortar mix proportions

	Proportion by weight
Cement	2
Sand	6
Water	1

addition its high value of Young's Modulus, in contrast to that of acrylate which is negligible, means that the theoretical analysis of the strains in the fibre/coating composite will be much more complicated.

FBGs are a specific kind of fibre sensor that consists of a length of fibre where the refractive index is changed in a periodic manner. This forms a number of micro-cavities which reflect light at their resonant wavelength. The Bragg wavelength of such a device is given by:

$$\lambda_B = 2n_{eff}\Lambda \tag{3}$$

where Λ is the period of the refractive index variation and n_{eff} is the weighted average of the refractive index across the length of the grating.

In analogy to a trombone, as the fibre is stretched the "pitch" (frequency) of the light changes and thus the strain can be measured by measuring the "pitch" of the light. In practice, λ_B is not the parameter measured, but rather the wavelength at which the reflectivity drops by a certain value, e.g. 3 dB. As $\frac{d\lambda_B}{\lambda_B} = \frac{d\lambda}{\lambda}$ for any λ of the grating spectrum, no correction is needed. This method provides greater accuracy as, by fabricating the gratings so that the amplitude of the refractive index variation varies across the length of the grating, the gratings can be designed to have very sharp transition zones between the highly reflective resonant peak and the unreflective non-resonant background. The use of an FBG for sensing is illustrated in Fig. 1.

The corresponding differential equation to Eq. (3) is:

$$\frac{d\lambda}{\lambda} = \frac{\frac{\partial n_{eff}}{\partial \sigma}d\sigma + \frac{\partial n_{eff}}{\partial T}dT}{n_{eff}} + \frac{\frac{\partial \Lambda}{\partial \sigma}d\sigma + \frac{\partial \Lambda}{\partial T}dT}{\Lambda} = (1+n_\sigma)d\sigma + n_T dT + \alpha dT \tag{4}$$

where $\alpha = \frac{1}{\Lambda}\frac{\partial \Lambda}{\partial T}$, $n_T = \frac{1}{n_{eff}}\frac{\partial n_{eff}}{\partial T}$ and $n_\sigma = \frac{1}{n_{eff}}\frac{\partial n_{eff}}{\partial \sigma}$ are the thermal expansion, thermo-optic and elasto-optic coefficients of fused silica glass, given as $5.5*10^{-7}$ K^{-1}, $8.11*10^{-6}$ K^{-1} and -0.22, respectively. These constants are all well documented by Corning and other manufacturers of fibre optic cable and they provide a highly accurate means of calibrating the sensor.

Table 2
RPC mix proportions

	Proportion by weight
Cement	340
Silica fume	102
Silica flour	102
Sand	487
Steel fibres	78
Water	75
Superplasticiser	24

Fig. 2. Experimental setup.

Fibre optic sensors have been used previously to measure the coefficient of thermal expansion of mortar and concrete [14]; however this was performed with a Michelson interferometer rather than FBG sensors. For the FBG sensor, only the strain from the grating region is measured. For the Michelson interferometer, the whole length of fibre is the sensor and as such the sensor will detect the fringing effects of temperature towards the surface of the specimen [15] as well as the inevitable temperature differences between the fibres leading in and out of the concrete. Thus such sensors can provide only a semi-empirical measurement of the internal strain and temperature effects rather than being able to function as a completely empirical measurement system.

Using FBG optical fibre sensors for measuring the thermal effects of cementitious materials offers submicrostrain accuracy independent of gauge length. This is because the gauge length for an FBG is a fixed value equal to its period, $\Lambda \approx 0.53$ μm. Unlike conventional sensors, with an FBG the gauge length is not the length to which measurement is limited. Rather an FBG consists of thousands of approximately 0.53 μm sensing regions which compose the whole length of the grating. The response of the FBG is due to a composite of the responses of all these sensing regions. Thus sensing with an FBG can be both representative of the bulk behaviour of the sample (provided the length of the grating is large compared to the coarsest grade of the aggregate) as well as giving the ability to monitor strains that are localised to the order of half a micron using more advanced sensing techniques. This is achieved using an optical pulse-echo technique, similar to that of acoustic imaging, so as to isolate the effects that occur within the single gauge length regions.

Another advantage of optical sensors is provided by the ability to embed them in a non-invasive manner (the coated fibre is 250 μm in diameter). This means that the internal bulk characteristics of a material can be monitored as well as the surface effects. Furthermore, fibre optic sensors exhibit virtually no long term drift and because they are a pure optical rather than an electrical measurement, they can operate in an aqueous environment as well as being immune to electromagnetic

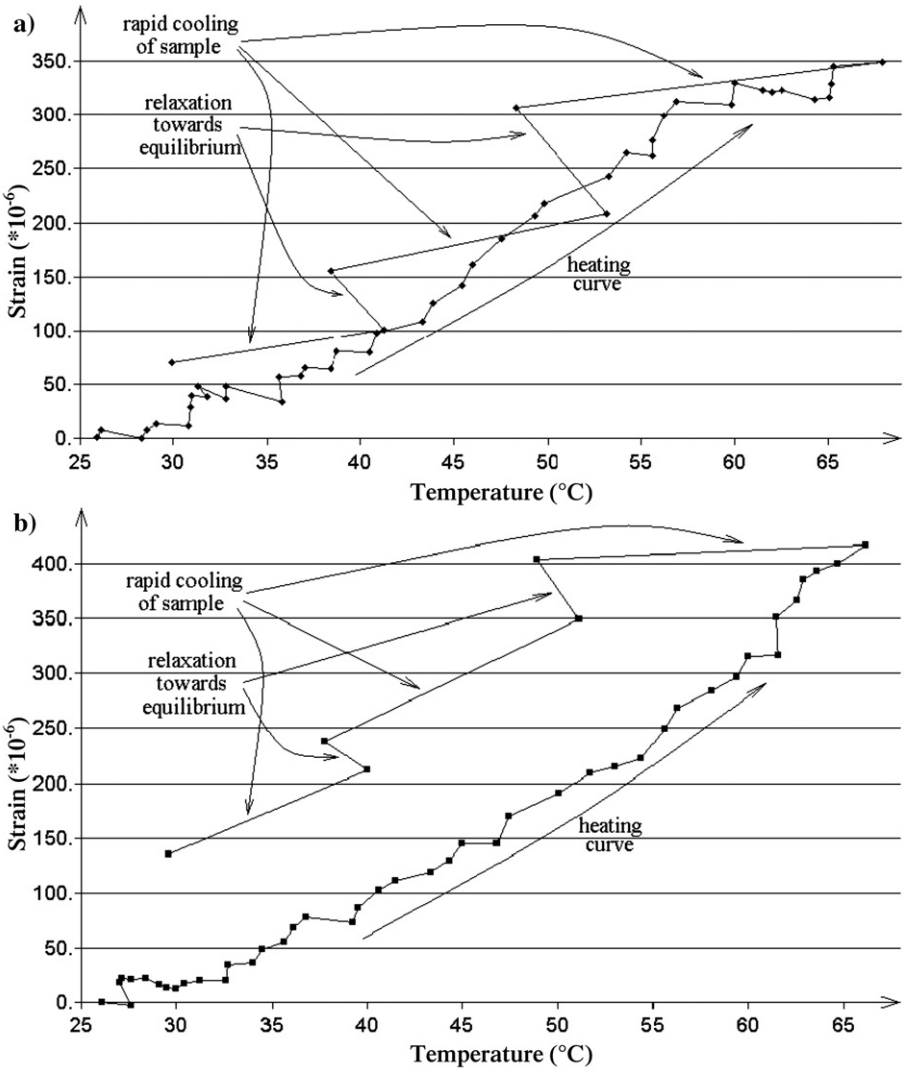

Fig. 3. Full heating and cooling curve of test 2 for the mortar prism (a) and the RPC prism (b) showing the deviation from linearity when cooling too rapidly for thermal equilibrium to be maintained.

interference. However, for our purpose the main advantage is that of being able to measure the samples under test as they are being heated, thus allowing the rapid collection of a large amount of data in a short period of time.

2. Experiment

Five fibre Bragg gratings having resonant wavelengths of 1523.7 nm, 1524.2 nm, 1523.9 nm, 1538.7 nm and 1555.8 nm were fabricated in a highly photosensitive boron codoped germanosilicate fibre at the UNSW fibre Bragg grating writing facility. The gratings were annealed to a thermal age of 20 years to ensure stability and left overnight in an oven at 80 °C in order to outgas the excess hydrogen used to increase the photosensitivity. The gratings were then recoated with acrylate to protect the glass fibre against the high pH of the cementitious mix. Using moulds that measured 25 × 25 × 280 mm, the former two gratings were embedded into a mortar mix given in Table 1. The latter three gratings were embedded into a RPC mix given in Table 2. The cement used was a GP Portland cement compliant with AS3972. The silica fume was a Western Australian undensified silica fume, the silica flour was graded at 300 G (i.e. with a maximum of 5% of the particles greater than 53 μm) and the sand used was Sydney sand. The steel fibres used had a length of 13 mm and a diameter of 0.2 mm and a Glenium 51 superplasticiser was chosen for use as the water reducer. Earlier embedding tests had shown that the fibres embedded into the RPC were highly susceptible to breakage at the surface due to the stiffness of the RPC. To avoid this, a small amount of bluetak was applied around the fibre at the point where it protruded from the RPC. The specimens were cured under standard moist conditions for 7 days and then left for 28 days to dry according to AS1012.8.1 clause 9 (2000) [16] and AS1012.13 subclause 7.3 [17]. This was all done so as to comply with the requirements for monitoring the drying shrinkage of the specimens so that the performance of the optical sensors in these specimens could be guaranteed prior to the thermal tests. The prisms were placed in a water bath, each supported by 2 pairs of stacked glass plates in order to reduce the effect of friction, and thus allow slippage between the

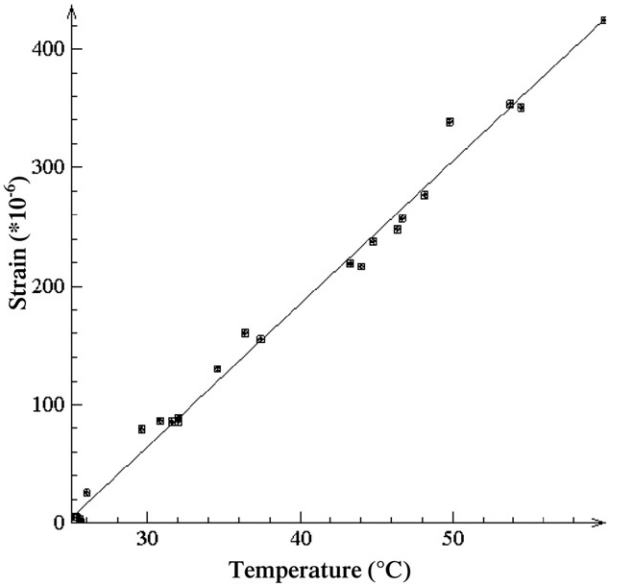

Fig. 4. Thermal expansion of the mortar prism during test no. 1.

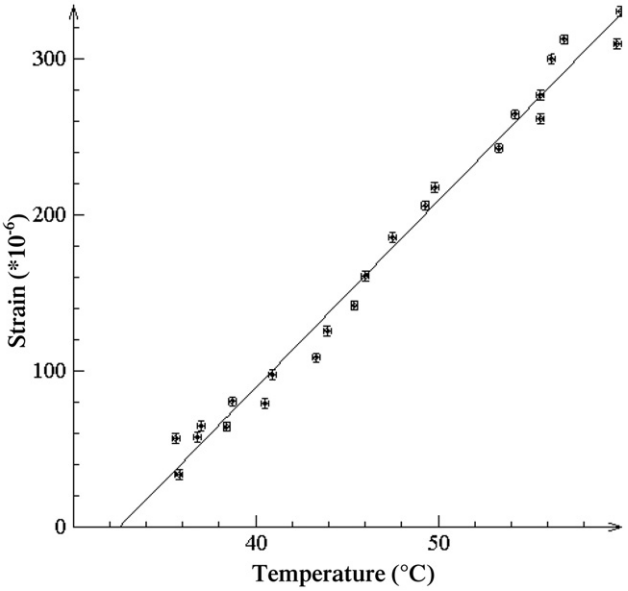

Fig. 6. Thermal expansion of the mortar prism during test no. 3.

concrete prism and the bottom of the water bath. Thermocouples were used to monitor the temperature of the water surrounding each prism (see Fig. 2).

Four tests were performed; the first was performed using the first mortar prism at an average heating rate of 0.2 K/min. The second was performed using the second mortar prism and the third RPC prism at an average heating rate of 0.7 K/min. The third test was performed using the second mortar prism and the second RPC prism at an average heating rate of 1.1 K/min. The fourth test was performed using the first RPC prism at an average heating rate of 0.4 K/min. The temperature range was kept within the range from 20 °C to 80 °C as above 80 °C the reliability of the bonding of the PMMA coating of the fibres to the cementitious matrix is questionable. Furthermore in using a water bath, agitation of the water as it approaches its boiling point introduces strain noise in the system, reducing the reliability of the data. An oil bath circumvents this problem but as it eats away at the bluetak, it is not worth the risk of snapping the fibres at the surface of the RPC specimens during testing. Using mercury as the liquid to heat the samples [18] is extremely hazardous and thus unsuitable. Data readings for the first four minutes of the test showed an abnormal amount of deviation from linearity. Two effects likely to cause this are the initial percolation of water through the prisms and having a residual amount of tension on the fibre from the drying shrinkage. Percolation of water would cause swelling giving an apparent effect equivalent to that of an increase in temperature. It would be significantly slower and smaller for the RPC prisms due to

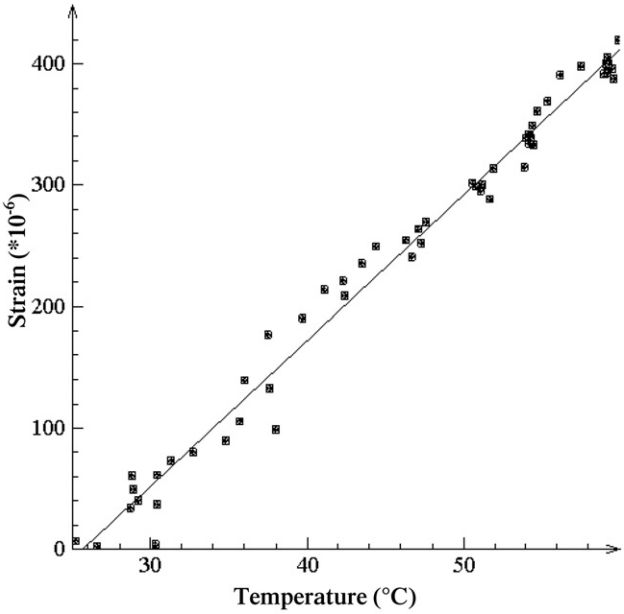

Fig. 5. Thermal expansion of the mortar prism during test no. 2.

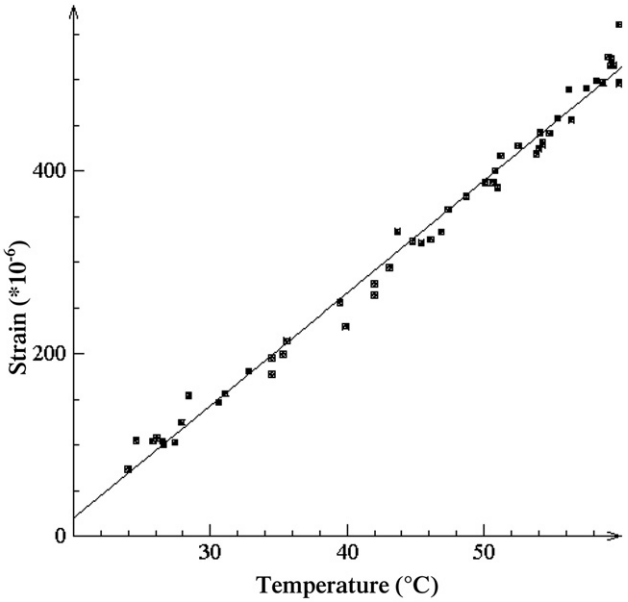

Fig. 7. Thermal expansion of the RPC prism during test no. 2.

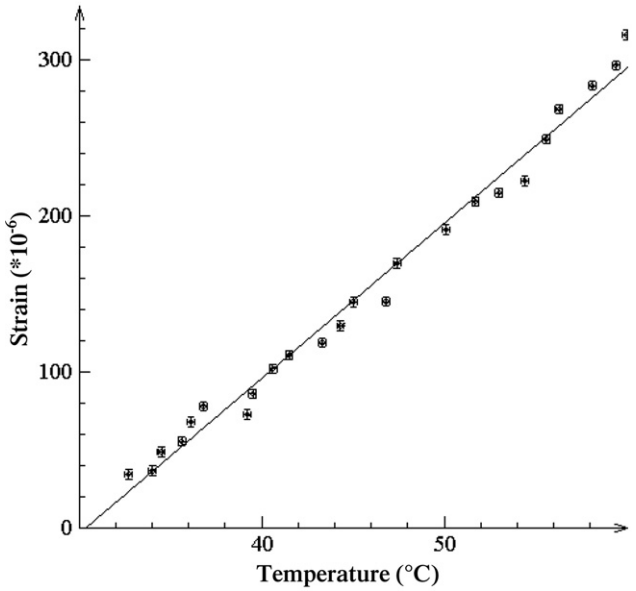

Fig. 8. Thermal expansion for the RPC prism during test no. 3.

their much lower porosity compared to the mortar prisms. This however is not the case. In most cases the deviation was instead equivalent to an apparent decrease in temperature. The effect varied strongly from sample to sample and the prism with the largest apparent increase in temperature was actually an RPC prism rather than a mortar prism. All of this evidence indicates that the effect is most likely due to residual strain rather than water percolation. In order to obtain a more accurate value for the CTE it was decided to exclude these measurements, along with those due to temperatures in excess of 60 °C (as was the practice in [5,6]), when fitting a trend to the data. For temperatures above 60 °C the CTE begins to deviate slightly from the value for normal operating temperatures of concrete.

In calculating the thermal strain of the prism, it is necessary to compensate for a variety of effects in the fibre. Firstly, the increase in temperature will cause a change in the refractive index of the fibre, n_{eff}, due to the thermo-optic effect. Secondly, due to the bonding between the fibre and the host material, the difference between the thermal expansivities must be taken up by the strain of the fibre. There will likewise be some strain acting on the host material; however, due to its size in comparison to the fibre, this will be negligible. This strain will cause a change in the period, Λ, of the Bragg grating as well as being accompanied by a change in the refractive index of the fibre due to the elasto-optic effect. Both of these will act to change the wavelength of the grating according to Eq. (4). In considering all of these effects, the resultant thermal strain of the prism, $dl/l = d\sigma + \alpha dT$, is given as:

$$\frac{d\lambda}{\lambda} = (1+n_\sigma)\left(\frac{dl}{l} - \alpha dT\right) + n_T dT + \alpha dT \tag{5}$$

$$\frac{dl}{l} = \frac{d\lambda/\lambda + (\alpha n_\sigma - n_T)dT}{1+n_\sigma}\ . \tag{6}$$

The equation giving the relative error associated with determining the CTE using optical measurements alone for the same temperature scale is found similarly to Eq. (2) as:

$$\frac{dC}{C} = 4\frac{1+n_\sigma}{(n_T+\alpha)}\frac{d\varepsilon}{\Delta T} = 0.0066, \tag{7}$$

where dε, the error in measuring strain, has been conservatively taken as 1 με [7]. This gives a relative error of 0.66% which is an order of magnitude improvement over the accuracy of that of mechanical measurements as was derived from Eq. (2).

3. Results and discussion

The full heating/cooling curve of test 2 is shown in Fig. 3a and b for the mortar prism and the RPC prism respectively. The large apparent thermal hysteresis of the RPC prism, which can be seen by the cooling curve having deviated from that of the path traced by the heating curve, shows that the RPC prism has a much larger heat capacity than that of the mortar prism. This is likely due to the much lower porosity of the RPC as compared to that of the mortar. Having a lower porosity reduces the ability to transport heat through the pore system.

The failure of the curve to come anywhere near doubling back on itself with the cooling rate of 2.77 K/min used in this test suggests that the heating rate of 1.1 K/min that was used in the third test will be too fast to ensure that thermal equilibrium is achieved for the RPC prism for the whole duration of test, thus leading to an error involved in evaluating the thermal expansion of the RPC. As the prism is cooler than the displayed temperature, this will lead to an underestimation of the coefficient of thermal expansion. The agreement of the results for the second and fourth tests despite the differences in heating rates show that the RPC prism maintained a sufficient level of thermal equilibrium for the duration of both tests and as a result the coefficient of thermal expansion that was evaluated will be accurate for both cases.

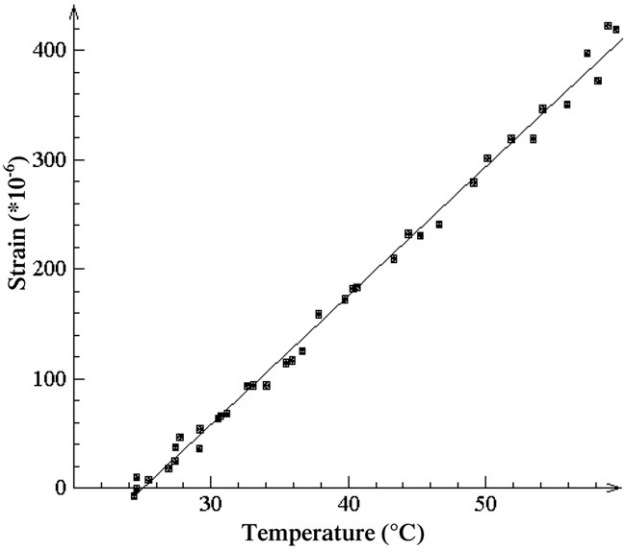

Fig. 9. Thermal expansion for the RPC prism during test no. 4.

Table 3
Coefficient of thermal expansion for differing material types and heating rates

Heating rate (K/min)	CTE of mortar ($*10^{-6}$ K^{-1})	CTE of RPC ($*10^{-6}$ K^{-1})
0.2	12.03±0.06	
0.4		11.76±0.04
0.7	11.98±0.04	12.33±0.04
1.1	11.96±0.08	9.93±0.07

The derived thermal strain of the mortar prisms for tests 1–3 and that of the RPC prisms for tests 2–4 are shown in Figs. 4–9 respectively. The calculated thermal expansion coefficients in these tests are shown in Table 3 for the various heating rates and two material types. Error values have been calculated from standard linear regression analysis. The result for the RPC prism when the heating rate reaches 1.1 K/min shows that the CTE has been underestimated for this case as has been stated above. Excepting this, the values compare well with those found in the literature [19–21] and their associated error values with what was calculated in Eq. (7).

The measured data are closely bunched around the calculated least mean squares fits, the correlation being 98% or better in all cases. The data points that show the most deviation from linearity occur largely in regions where the heating rate is higher than the average, evidenced by the points being more spread apart with temperature. As such it is expected that higher accuracy is possible by means of having, not just a slow heating rate on average, but one that is consistently so.

4. Conclusions

The thermal expansion of the mortar prisms was found to be $(12.03\pm0.06)*10^{-6}$ K^{-1} and $(11.98\pm0.04)*10^{-6}$ K^{-1}. The thermal expansion of the RPC prisms was found to be $(11.76\pm0.04)*10^{-6}$ K^{-1} and $(12.33\pm0.04)*10^{-6}$ K^{-1}. The data obtained from the FBG sensors was well correlated with the fitted linear regressions and the obtained coefficient of thermal expansion was in good agreement with previously observed results. The use of fibre optic sensing was shown to give an order of magnitude improvement in the accuracy of measurement as compared to what is attainable using conventional sensing techniques.

Acknowledgements

This work was supported in part by an APAI grant courtesy of the Australian Research Council and the Roads and Traffic Authority, NSW, Australia.

References

[1] K.D. Hertz, Limits of spalling of fire exposed concrete, Fire Saf. J. 38 (2003) 103–116.
[2] K.D. Hertz, L.S. Sørenson, Test method for spalling of fire exposed concrete, Fire Saf. J. 40 (2005) 466–476.
[3] A.S. Usmani, N.J.K. Cameron, Limit capacity of laterally restrained reinforced concrete floor slabs in fire, Cem. Concr. Compos. 26 (2004) 127–140.
[4] J.C.C. da Silva, C. Martelli, H.J. Kalinowski, E. Penner, J. Canning, N. Groothoff, Dynamic analysis and temperature measurements of concrete cantilever beam using fibre optic sensor, Opt. Lasers Eng. 45 (2007) 88–92.
[5] U.S. Army Corps of Engineers, Test method for coefficient of linear thermal expansion of concrete, CRD-C 39-81, Handbook for Concrete and Cement, Miss., Vicksburg, 1997.
[6] U.S. Army Corps of Engineers, Method of test for coefficient of thermal expansion of mortar, CRD-C 126-63, Handbook for Concrete and Cement, Miss., Vicksburg, 1997.
[7] A.D. Kersey, M.A. Davis, H.J. Patrick, M. LeBlanc, K.P. Koo, C.G. Askins, M.A. Putnam, E.J. Friebele, Fiber grating sensors, J. Lightwave Technol. 15 (1997) 1442–1463.
[8] Byoungho Lee, Review of the present status of optical fiber sensors, Opt. Fiber Technol. 9 (2003) 57–79.
[9] C.I. Merzbacher, A.D. Kersey, E.J. Friebele, Fiber optic sensors in concrete structures: a review, Smart Mater. Struct. 5 (1996) 196–208.
[10] V. Slowik, E. Schlattner, T. Klink, Experimental investigation into early age shrinkage of cement paste by using fibre Bragg gratings, Cem. Concr. Compos. 26 (2004) 473–479.
[11] R. Maaskant, T. Alavie, R.M. Measures, G. Tadros, S.H. Rizkalla, A. Guha-Thakurtad, Fiber-optic Bragg grating sensors for bridge monitoring, Cem. Concr. Compos. 19 (1997) 21–33.
[12] M.A. Davis, D.G. Bellemore, A.D. Kersey, Distributed fiber Bragg grating strain sensing in reinforced concrete structural components, Cem. Concr. Compos. 19 (1997) 45–57.
[13] E. Karamehmedović, P. Childs, T. Whitbread, A.C.L. Wong, N. Gowripalan, G.D. Peng, Field test of strain fluctuation in the experimental reactive powder concrete bridge at Shepherd's Creek, PROC ACOFT, 2005, pp. 543–545.
[14] Q. Li, L. Yuan, F. Ansari, Model for measurement of thermal expansion coefficient of concrete by fiber optic sensor, Int. J. Solids Struct. 39 (2002) 2927–2937.
[15] L. Yuan, W. Jin, L. Zhou, K. Lau, The temperature characteristic of fibre-optic pre-embedded concrete bar sensor, Sens. Actuators, A 93 (2001) 206–213.
[16] Standards Australia, AS1012.8.1, Methods of Testing Concrete, Method 8.1: Method for Making and Curing Concrete — Compression and Indirect Tensile Specimens, 2000.
[17] Standards Australia, AS1012.13, Methods of Testing Concrete, Method 13: Determination of the Drying Shrinkage of Concrete for Samples Prepared in the Field or in the Laboratory, 1992.
[18] S. Sabri, J.M. Illston, Immediate and delayed thermal expansion of hardened cement paste, Cem. Concr. Res. 12 (1982) 199–208.
[19] A.M. Neville, Properties of concrete, 4th edn. Longman, Essex, 1995.
[20] F. Vodák, R. Černỳ, J. Drchalová, Š. Hošková, O. Kapičková, O. Michalko, P. Semerák, J. Toman, Thermophysical properties of concrete for nuclear-safety related structures, Cem. Concr. Res. 27 (1997) 415–426.
[21] J.-H.J. Kim, S.-E. Jeon, J.K. Kim, Development of new device for measuring thermal stresses, Cem. Concr. Res. 32 (2002) 1645–1651.